Latin American Journal of Solids and Structures
www.lajss.org

Three-Dimensional Determination of Superposed Helical Wires Constraint Ability

Abstract
A three-dimensional theoretical model for predicting the maximum force sustained by a flexible line wound around a rigid cylindrical body is developed based on Clebsch-Kirchhoff equilibrium equations, considering its bending rigidity, no sliding, modified non-linear frictional law in terms of stress and an external pressure exerted on the line. Likewise, this model is extended to solve the constraint problem of superposed counter wound helical wires. Results given by 4th order Runge-Kutta numerical algorithm show that, except for the line thickness, the constraint ability grows with an increase of other geometric parameters and external pressure. However, it cannot be significantly enhanced by applying external pressure for large initial forces, especially when there is an initial binormal force.

Keywords
constraint ability; capstan effect; nonlinear frictional law; superposed helical wires

Junpeng Liu [a*]
Murilo Augusto Vaz [b]

[*a] Institute for Ocean Engineering, China University of Petroleum (Beijing), Beijing, China. Email: liujpcup@gmail.com

[b] Ocean Engineering Program, Federal University of Rio de Janeiro, Rio de Janeiro, Brazil. Email: murilo@oceanica.ufrj.br

*Corresponding author

http://dx.doi.org/10.1590/1679-78254085

Received: June 05, 2017
In Revised Form: September 08, 2017
Accepted: December 08, 2017
Available online: February 05, 2018

1 INTRODUCTION

Flexible lines, such as wires, ropes or fibers, wound around cylindrical body, are capable of making up some useful devices in engineering applications. The most likely device called capstan is used aboard ships or rope rescue systems, see Figure 1-A, to control a rope under significant tension. Besides, another very common device is thermoplastic wire hose which is unique in its ability to undergo large internal pressure. The basic construction configuration consists of an inner core with layers of helical wires, as seen in Figure 1-B. In order to achieve a torque stable design, the wire layers are wound in pairs at opposite directions. When an internal pressure is exerted on a hose, apparently, the helical wire will be subjected to nearly equal tension stresses along its arc length with no slide, preventing the inner core to expand radially. However, once the tension force on the wire exceeds the maximum value that can be held due to the capstan effect, the wires will slide. This maximum force is henceforth defined as the constraint force. Similar constructions can also be found in flexible pipes which are widely used in the offshore industry for oil and gas extraction from subsea reservoirs, and many efforts have been carried out to deal with the structural analysis of the armor layers of flexible pipes [1-4]. For all these kinds of structures, estimating the constraint force and then evaluating the constraint ability are important to ensure their functional integrity.

Classical capstan formula, referred to as Euler's equation of tension transmission, relating the loading force F_{loading} to the hold force $F_{holding}$ applied at two ends of the rope is expressed as: $F_{loading} = F_{holding} e^{\mu\theta}$, where μ is the coefficient of friction and θ denotes the contact angle of a cable wrapped around a capstan, illustrated in Figure 1-C. This equation can be used to calculate the constraint force in capstan problem and it is obvious that a hold-force can resist a much higher load-force due to the friction which increases exponentially with the friction coefficient and the contact angle.

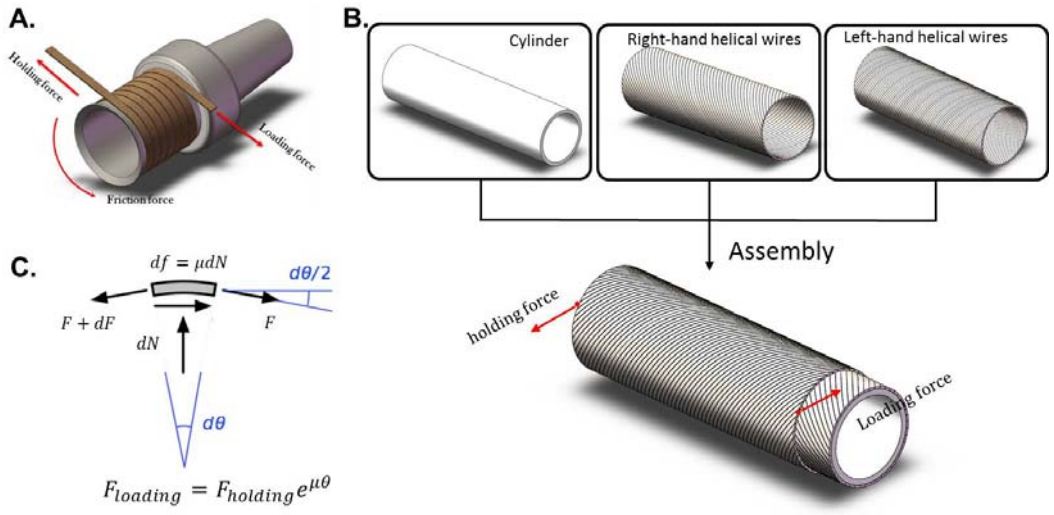

Figure 1: *Examples of devices based on capstan effect and classical capstan equation diagram*

In spite of the fact that the Euler's equation can be readily employed to analyze the mechanical behavior of flexible lines in contact with circular profiled surfaces [5-8], it shares many of the following idealized hypotheses, which significantly limit the applicability range of the results: frictional coefficient is constant in the entire wire; flexible line does not have bending rigidity; no deformation occurs when loads are applied on both ends.

To improve the equation's practicality, many research studies have been carried out. With a combination of experiment and classical capstan equation, Martin and Mittelmann [9] pointed out that the frictional coefficient of the wool fiber approximately reduces up to 50%, if the initial tension is increased. Such interesting phenomenon has drawn attention and motivated research to confirm and explain it. Most interpretations are based on empirical approaches, but conclusion about friction drop behavior has been gradually accepted in many areas such as polymer and tribology. In order to overcome the limitations induced by empirical work, Howell [10, 11] presented a non-linear relationship between frictional and normal forces, however, the fact that the effects of bending rigidity were neglected and the relation between friction and capstan's radius was not shown limited its reliability. Brown and Burgoyne [12] put forward a modified version of Howell's equation in terms of stress, which was used to study the friction and wear behavior of Kevlar 49. Stuart [13] studied the capstan problem of strings considering the bending rigidity. Similarly, Wei and Chen [14] conducted an approximate theoretical analysis of the tension increase for nonflexible fibers and yarns passing around a peg. Jung et al. [15] derived a generalized capstan equation with bending rigidity to explain the tension transmission of an elastic rod gripped by two circular-edged plates in the contact region. The same authors [16] improved the classical capstan equation by adding the rod bending rigidity and a power-law friction. Parametric analysis showed both parameters played a significant influence on the tension ratio. On the authority of previous model, they [17] also addressed a more comprehensive study considering two other factors: extensibility and the Poisson's effect. Gao et al. [18] proposed a modified capstan equation including bending rigidity and power-law friction effects, and compared numerical and experimental results. Liu and Vaz [19] described the constraint ability of superposed woven fabrics wound on capstan by updating the classical capstan equation under such considerations: modified frictional law in terms of stress and external pressure.

Most of previous work has focused on two-dimensional model comprehensively concerned on tension transmission in capstan problems, but little attention has been paid to the lateral constraint force which may play an important role in engineering design. Moreover, it should be noted that external pressure exerted on the flexible line is common for thermoplastic wire reinforced hoses or flexible pipes. Besides, it is easy to imagine that mechanically applying external pressure can effectively improve the constraint ability. However, attempts to quantify the effect of external pressure on the capstan problem have not yet been highlighted. Therefore, the objective of this study is to combine the effects of wire's bending rigidity, non-linear friction law and external pressure in a three-dimensional model for capstan problem employing Clebsch-Kirchhoff equilibrium equations for a spatial rod to accurately generate the helical wire constraint force as a function of its arc length. Furthermore, this three-dimensional model also leads to a method to determine the constrain ability of superposed layers. Likewise, in this paper, observations from a comprehensive case study indicate the most influential parameters in the model.

2 MATHEMATICAL MODEL

Consider an idealized three-dimensional helical configuration shown in Figure 2. The wire cross-section is usually circular or rectangular (in this paper, the cross-section is assumed rectangular with thickness H and width W), being wound with a helical angle α around a rigid cylinder whose radius is R. As a consequence from friction force between wire and cylinder contact surfaces the wire can remain fixed. In order to establish the distribution of the maximum force sustained by the wire, consider a local coordinate system where **t, b, n** respectively represent tangential, binormal and normal directions. When the wire is subjected to a force generated by device or resulting from internal pressure, a critical force F must not be exceeded to avoid the wire slip.

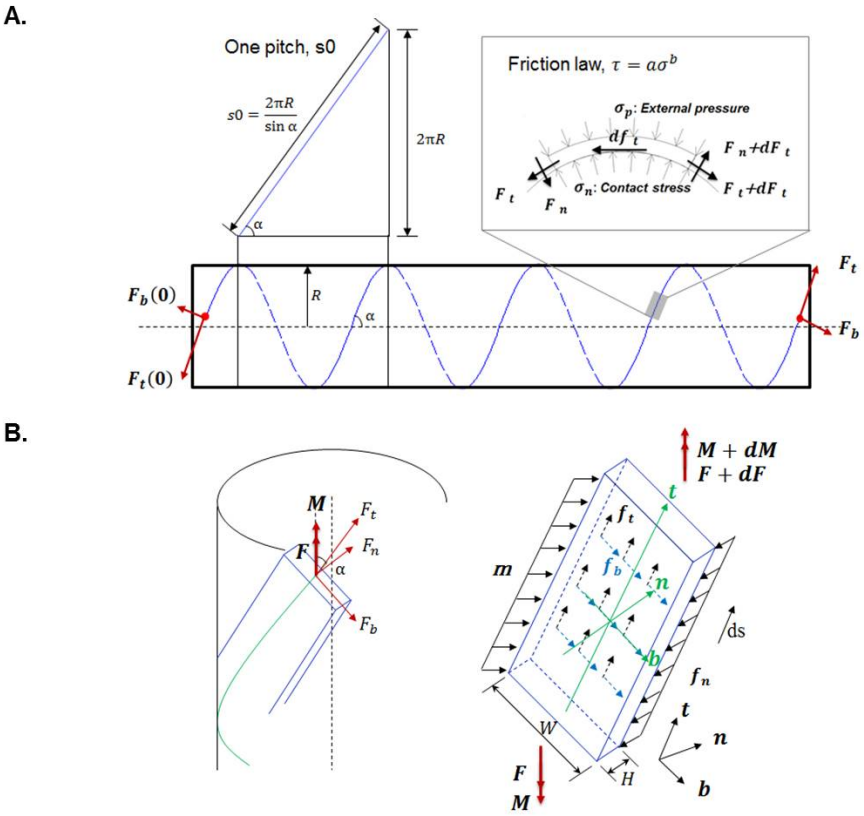

Figure 2: *Diagram of a single wire wound around a rigid cylinder (A: a pitch is defined as s0 and friction law is introduced; B: local coordinate system and curved wire equilibrium.)*

It is clear that, in addition to tangential force F_t dominating the wire equilibrium status, stick or slip, another relevant component is binormal force F_b which is important to determine whether the wire can slip. Note that an arc length dependent force acts on the wire causing the helical angle to vary. Given this variation is often relatively small, for the purpose of a simplified analysis let the helical angle α be constant. Moreover, attention is confined to systems assumed geometric linearity.

Geometry

The curvature components k_t, k_n, k_b for a wire shown in Figure 2 can be written as:

$$k_t = \frac{\sin 2\alpha}{2R}$$
$$k_n = \frac{(\sin\alpha)^2}{R} \qquad (1)$$
$$k_b = 0$$

where the subscripts t, n, b respectively denote tangential, normal and binormal directions.

Force analysis

The equilibrium equations for long slender curved rods (Love [20] and Reissner [21]) have a wide range of applications in applied mechanics:

$$\frac{dF}{ds}+ f = 0,\ \frac{dM}{ds}+t\times F + m = 0 \tag{2}$$

where $\boldsymbol{f}$ and $\boldsymbol{m}$ respectively denote the distributed friction force and moment.

Substitution of loads and curvature components in local coordinate system into Eq.(2) gives the Clebsch-Kirchhoff equilibrium equations:

$$\frac{dF_t}{ds} - k_n F_n + k_b F_b + f_t = 0 \tag{a}$$

$$\frac{dF_n}{ds} + k_n F_t - k_t F_b + f_n = 0 \tag{b}$$

$$\frac{dF_b}{ds} - k_b F_t + k_t F_n + f_b \tag{c}$$

$$\frac{dM_t}{ds} - k_n M_n + k_b M_b + m_t = 0 \tag{d}$$

$$\frac{dM_n}{ds} + k_n M_t - k_t M_b - F_b + m_n = 0 \tag{e}$$

$$\frac{dM_b}{ds} - k_b M_t + k_t M_n + F_n + m_b = 0 \tag{f}$$

Let E and G respectively be the elastic and shear moduli, so the bending moment components on the cylinder cross-section in terms of corresponding stiffness and curvature variations are given by:

$$\begin{aligned} M_t &= GI_t \Delta k_t \\ M_n &= EI_n \Delta k_b \\ M_b &= EI_b \Delta k_n \end{aligned} \tag{4}$$

Disregarding change in the initial wire configuration yields, $\Delta k_t = \Delta k_n = \Delta k_b = 0$ thus Eq.(4) becomes:

$$M_t = M_n = M_b = 0 \tag{5}$$

Therefore:

$$\frac{dM_n}{ds} = \frac{dM_b}{ds} = \frac{dM_t}{ds} = 0 \tag{6}$$

As the distributed friction force $\boldsymbol{f}$ exists, there must be moment balance in the wire cross-section. Although the normal distributed moment is difficult to envisage, the other two components can be expressed in the form:

$$m_t = -f_b . \frac{H}{2} \tag{a}$$

$$m_b = -f_t . \frac{H}{2} \tag{b} \tag{7}$$

When Eq.(5) and (6) are substituted into Eq.(3-d), the tangential distributed moment m_t is zero, implying that there is no distributed friction force in binormal direction, i.e. f_b=0.

Friction law

In this paper, a non-linear friction law in terms of stress is taken into consideration. Suppose the contact pressure between wire and cylinder is σ, which is the sum of tension-dependent pressure component σ_n and tension-independent pressure (or external pressure) σ_p as shown in Figure2-A. Let *a* and *b* correspond to material friction constants which are experimentally determined, and friction stress is characterized by $\tau \le a\sigma^b$ (stick) or $\tau = a\sigma^b$ (slip), so the distributed normal force f_n and friction force f_t are respectively given by:

$$f_n = -\sigma_n W \quad \text{(a)}$$

$$f_t = -a(\sigma_n + \sigma_p)^b W \quad \text{(b)} \quad (8)$$

where both σ_n and σ_p are the absolute value of the pressure.

Constraint force components - arc length relation

Expressions for the force components, found by substituting Eq.(5), (6), (7) and (8) into Eq.(3), are:

$$\frac{dF_t}{ds} = \left[\frac{(\sin\alpha)^2}{R} - \frac{2}{H}\right] F_n \quad \text{(a)}$$

$$\frac{dF_n}{ds} = -\frac{(\sin\alpha)^2}{R} F_t + W\left(-\frac{2}{aWH} F_n\right)^{\frac{1}{b}} + \frac{\sin 2\alpha}{2R} F_b - \sigma_p W \quad \text{(b)}$$

$$\frac{dF_b}{ds} = -\frac{\sin 2\alpha}{2R} F_n \quad \text{(c)} \quad (9)$$

To solve this set of differential equations, initial conditions are assumed to be:

$$F_t|_{s=0} = F_t(0), \quad F_n|_{s=0} = F_n(0), \quad F_b|_{s=0} = F_b(0)$$

More generally, $F_t(0)$ is significantly larger than the other two. Considering engineering applications, several observations can be made about the constraint force components from Eq.(9):

1. As the value of $\left[(\sin\alpha)^2 / R - 2/H\right]$ is obviously less than zero, the value of normal force must be negative to ensure that the tangential constraint force increases along arc length. In fact, it is easy to understand this state in accordance with the normal direction supposed in the local coordinate system.
2. The interaction among the three constraint force components is complicated, which cannot be ruled directly by analytical expressions, except for particular cases.
3. The helical angle poses an important role on determining the growth of each force component. For instance, in Eq.(9-c), it affects the monotonicity of dF_b/ds and the critical point is at $\alpha = 45°$.
4. Additional information about the initial conditions and helical angle can be obtained from Eq.(9), by making use of $dF_n/ds < 0$:

$$\alpha > \alpha_{\min} = \frac{1}{2}\left\{\arcsin\left[\frac{F_t(0) - 2RW\left(-\frac{2}{aWH}F_n(0)\right)^{\frac{1}{b}} + W\sigma_p}{\sqrt{F_t(0)^2 + F_b(0)^2}}\right] - \arctan\left(\frac{F_t(0)}{F_b(0)}\right)\right\} \quad (10)$$

That is to say, once the initial conditions about the force components are given, in the process of engineering design, the helical angle must satisfy the requirements shown in Eq.(10). For cases without initial normal force and external pressure, i.e. $F_n(0) = 0$ and $\sigma_p = 0$, the minimum angle reduces to:

$$\alpha_{\min} = \arctan\left[\frac{F_b(0)}{F_t(0)}\right] \tag{11}$$

Next, consider the special case of linear friction law, i.e. *b=1*. Taking the derivative of Eq.(9-b) and combining Eq.(9-a,c), a second order differential equation in terms of normal force F_n is obtained:

$$\frac{d^2F_n}{ds^2} + \frac{2}{aH}\frac{dF_n}{ds} - \frac{(\sin\alpha)^2}{R}\left(\frac{2}{H} - \frac{1}{R}\right)F_n = 0 \tag{12}$$

Because the characteristic equation of Eq.(12) must have two real roots, $i.e. x_1, x_2 = -\frac{1}{aH} \pm \sqrt{\left(\frac{1}{aH}\right)^2 + \frac{(\sin\alpha)^2}{R}\left(\frac{2}{H} - \frac{1}{R}\right)}$, then the solution for normal force is given by:

$$F_n(s) = C_1 e^{x_1 s} + C_2 e^{x_2 s}$$

The constants C_1 and C_2 can be obtained through the following two initial conditions:

$$\begin{aligned} F_n|_{s=0} &= F_n(0) \\ \frac{dF_n}{ds}|_{s=0} &= -\frac{(\sin\alpha)^2}{R}F_t(0) + -\frac{2}{aH}F_n(0) + \frac{\sin\alpha.\cos\alpha}{R}F_b(0) - \sigma_p W \end{aligned} \tag{13}$$

Expressions for the tangential and binormal forces can be obtained by integrating Fn from the initial position 0 to s and considering the initial conditions, then multiplying the corresponding parameters shown in Eq.(9). Finally, the analytical solutions are:

$$F_t(s) = \left[\frac{(\sin\alpha)^2}{R} - \frac{2}{H}\right]\left(\frac{C_1}{x_1}e^{x_1 s} + \frac{C_2}{x_2}e^{x_2 s}\right) + C_3$$

$$F_b(s) = -\frac{\sin 2\alpha}{2R}\left(\frac{C_1}{x_1}e^{x_1 s} + \frac{C_2}{x_2}e^{x_2 s}\right) + C_4$$

Where C_3 and C_4 are constants determined by initial conditions: $F_t|_{s=0} = F_t(0)$ and $F_b|_{s=0} = F_b(0)$.

In summary, when the constraint force components are calculated through the three-dimensional model considering either linear frictional law or non-linear one, the constraint ability defined as tension transmission efficiency can be categorized into two classifications: tangential ratio and resultant force ratio, respectively, which can be expressed as:

$$\begin{aligned} T_t(s) &= \frac{F_t(s)}{F_t(0)} \\ T_r(s) &= \frac{\sqrt{F_t(s)^2 + F_n(s)^2 + F_b(s)^2}}{\sqrt{F_t(0)^2 + F_n(0)^2 + F_b(0)^2}} \end{aligned} \tag{14}$$

In addition, combining Eq.(3-f), (7-b) and (8-b), the normal force F_n can be written as:

$$F_n = -a(\sigma_n + \sigma_p)^b W.\frac{H}{2} \tag{15}$$

Hence, the contact stress σ_n in terms of F_n is found to be:

$$\sigma_n = \left(-\frac{2}{aWH} F_n \right)^{\frac{1}{b}} - \sigma_p \tag{16}$$

which is key information used in the following analysis.

In addition, a two-dimensional model for predicting the constraint ability of a traditional capstan device considering the bending rigidity and power-law friction effects can be easily deduced as a particular case from the three-dimensional model presented herein, based on the following assumptions:

1. The wrapping angle is φ, so $ds = Rd\varphi$

2. The curvature components respectively become $k_t = 0,\ k_n = \frac{1}{R},\ k_b = 0$.

3. Forces in binormal direction become zero.

Consequently, the relationship between the force components are:

$$\begin{aligned} &\frac{d^2F_t}{d\varphi^2} + \frac{2R}{H}\left(-\frac{H+2R}{2aR} \right)^{\frac{1}{b}} (WR)^{\frac{b-1}{b}} \left(\frac{dF_t}{d\varphi} \right)^{\frac{1}{b}} - \frac{2R}{H} F_t = 0 \\ &F_n = \frac{H}{2R}\frac{f_t}{d\varphi} = -\frac{H}{2R-H}\frac{dF_t}{d\varphi} \end{aligned} \tag{17}$$

It should be noted that Eq. (17) is similar to the equations (30) and (31) shown in Gao et al. [18], except the sign of F_n due to adopted directions. As experimental work performed in [18] has indicated the results show good agreement with formulation.

The constraint ability of superposed helical wires

When two layers consisting of several wires are wound in pairs with opposite angles and are assembled into a composite structure as shown in Fig 1-B, each wire in the internal layer contacts all wires in the external layer and the interaction of two layers influences the constraint abilities. Suppose that the near wires in each layer are so close that the contact stress is assumed continuous along arc length. In addition, the geometric parameters and frictional coefficients of each wire are assumed to be the same.

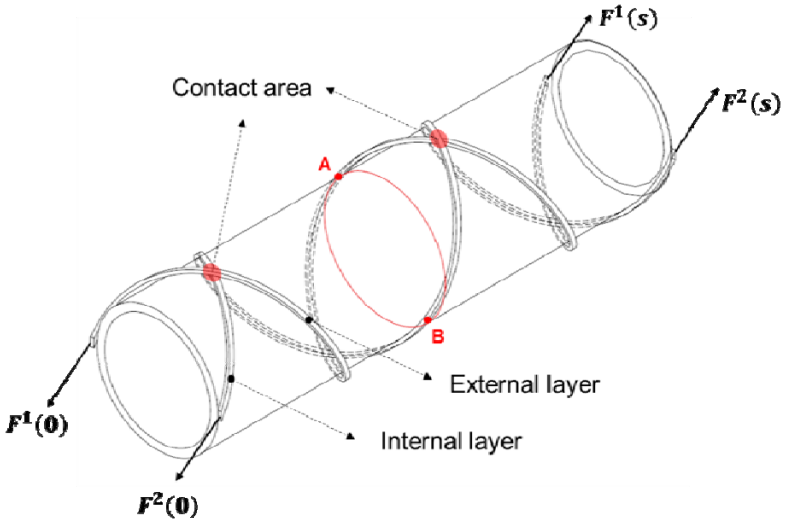

Figure 3: Diagram of one superposed helical wires

For convenience in presentation, it is common practice to choose two wires which are substantially symmetrical about the center from internal and external layers for analysis, as shown in Figure 3. Although the contact area between these two wires is small and discontinuous, given the geometric symmetry, the contact stress at point A generated by the external layer is equal to the stress acted on the internal layer at point B which plays a role of external pressure. That is to say, if the external wire is subjected to force, the contact stress σ_n along with its arc length must occur, which is equivalent to apply an external pressure on the internal wire.

Accordingly, using Eq.(9) and (16), the constraint ability of both external and internal wires can be obtained by the following differential equations:

$$\begin{aligned}
&\frac{dF_t^1}{ds}=\left[\frac{\left(\sin\alpha\right)^2}{R+H}-\frac{2}{H}\right]F_n^1\\
&\frac{dF_n^1}{ds}=-\frac{\left(\sin\alpha\right)^2}{R+H}F_t^1+W\left(-\frac{2}{aWH}F_n^1\right)^{\frac{1}{b}}+\frac{\sin 2\alpha}{2\left(R+H\right)}F_b^1-\sigma_p W\\
&\frac{dF_b^1}{ds}=-\frac{\sin 2\alpha}{2\left(R+H\right)}F_n^1\\
&\frac{dF_t^2}{ds}=\left[\frac{\left(\sin\alpha\right)^2}{R}-\frac{2}{H}\right]F_n^2\\
&\frac{dF_n^2}{ds}=-\frac{\left(\sin\alpha\right)^2}{R}F_t^2+W\left(-\frac{2}{aWH}\right)^{\frac{1}{b}}\left(F_n^2-F_n^1\right)^{\frac{1}{b}}+\frac{\sin 2\alpha}{2R}F_b^2+\sigma_p W\\
&\frac{dF_b^2}{ds}=-\frac{\sin 2\alpha}{2R}F_n^2
\end{aligned}\tag{18}$$

where superscripts 1 and 2 in force components respectively denote the external and internal layers, and the initial conditions are:

$$F_t^1\left|_{s=0}=F_t^1\left(0\right),\ F_n^1\right|_{s=0}=F_n^1\left(0\right),\ F_b^1\left|_{s=0}=F_b^1\left(0\right)\right.$$
$$F_t^2\left|_{s=0}=F_t^2\left(0\right),\ F_n^2\right|_{s=0}=F_n^2\left(0\right),\ F_b^2\left|_{s=0}=F_b^2\left(0\right)\right.$$

3 RESULTS AND DISCUSSIONS

The key to calculate the constraint ability of a single helical wire wound on a rigid cylinder is to obtain the maximum force that can be withstood by the wire for ensuring no slip. The force can be respectively decomposed into three components along tangential, binormal and normal directions, and the first two components are of interest in engineering applications. The first purpose of this section is to calculate constraint force components through the three-dimensional model mentioned above and discuss how those results differ from the ones obtained if bending rigidity is disregarded. The interaction among those three constraint force components as seen in Eq.(9) makes it a little difficult to distinguish parametric effects, to do so, case studies corresponding to numerous parameters such as geometry, friction and external force are performed. Moreover, it is shown that when a layer consisting of several wires is overlapped by another layer, its constraint ability is significantly increased. This is illustrated by considering two important sets of application: a single wire wound around a cylinder and two layers composed of several helical wires.

1) Single wire wound around rigid cylinder

Consider a helical wire and a cylinder which are assembled as shown in Figure 2. The helical wire has a rectangular cross-section (width W=0.03m and thickness H=0.005m) and is wound in a helical angle $\alpha=\pi/4$ around a cylinder whose radius is R=0.1m. The parameters related to friction law are assumed to be a=0.4 and b=0.9. Suppose that there is only one tangential force exerted on the wire at s=0, i.e. $F_t(0)=1$N, and $F_b(0)=F_n(0)=0$N.

Substituting the above parameters into Eq.(9) and using 4th order Runge-Kutta numerical method, results of constraint force components carried out with two external pressure cases, $\sigma_p=0$Pa and $\sigma_p=10$Pa are shown by solid lines in Figure 4.

In the previous model without considering wire bending rigidity, constraint forces in both normal and binormal directions are neglected due to their relatively small values. The expressions of tangential constraint force for linear and non-linear friction law ($b=1$ or $b\neq 1$) are [22]:

$$F_t(s)=\begin{cases}\dfrac{R}{a\sin^2\alpha}\left[e^{\frac{a\sin^2\alpha}{R}s+\ln\left(\frac{a\sin^2\alpha}{R}F_t(0)+aW\sigma_p\right)}-aW\sigma_p\right] & b=1\\ \dfrac{RW}{\sin^2\alpha}\left\{\left[a(1-b)\dfrac{\sin^2\alpha}{R}s+\left(\dfrac{\sin^2\alpha}{RW}F_t(0)+\sigma_p\right)^{(1-b)}\right]^{\frac{1}{1-b}}-\sigma p\right\} & b\neq 1\end{cases} \tag{19}$$

Combining the given parameters and Eq.(19), the dot lines in Figure 4 show the tangential constraint force which is larger than the one given by the model considering bending rigidity. Meanwhile, neither normal nor binormal forces are shown in Figure 4 as they are assumed to be zero in this model.

The largest difference between those two models is that the three-dimensional model has the ability to provide the normal and binormal constraint forces, although their values are very small, they are indeed capable of affecting the tangential force and are useful for engineering applications in which some accidental forces in normal or binormal directions are inevitable.

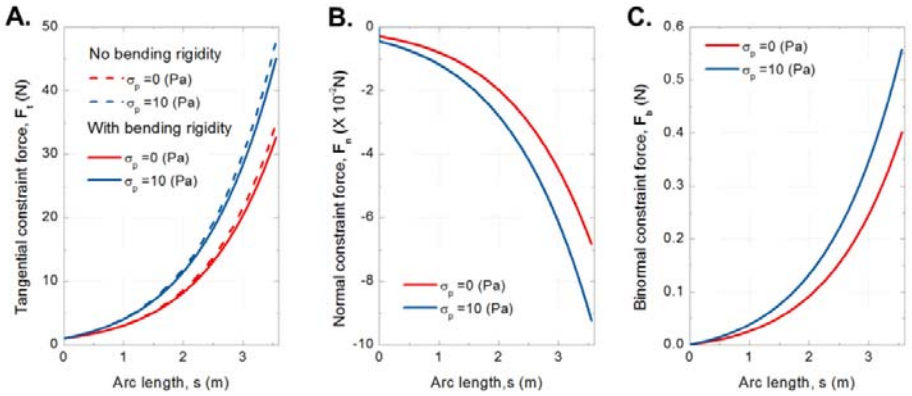

Figure 4: *Comparison of constraint force components generated by two different models (W=0.03m, H=0.005m, α=π/4, a=0.4, b=0.9,F_t (0) =1N, and $F_b(0)=F_n(0)=0$N)*

A smaller tangential force given by three-dimensional model may result because part of friction force is used to balance the normal and binormal forces. The diagram in Figure 4-B shows that the normal constraint force instantaneously increases from 0 to a certain value at s=0, taken from the numerical method where the gradient growth dF_n/ds is not zero at the first length step, and then grows gradually in absolute value. For the models considering or not the bending rigidity, the external pressure exerted on a wire is equivalent to increase the friction force. Consequently, the constraint ability must increase and changes in the position far from the initial point s=0 becomes more obvious.

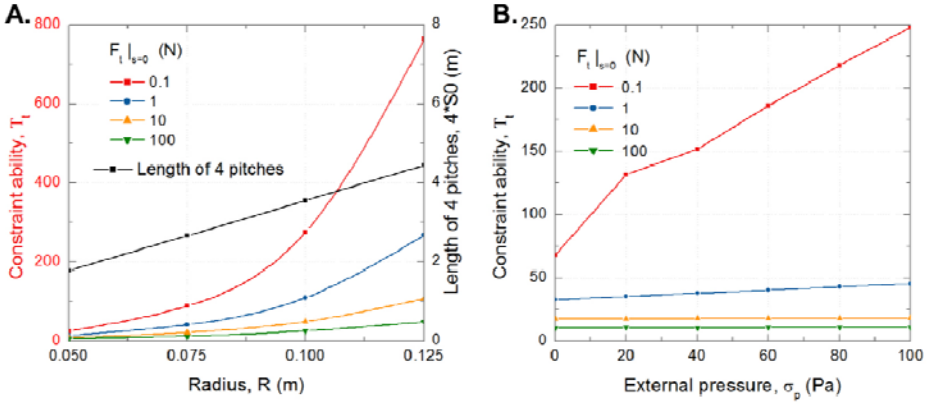

Figure 5: *Effect of initial force value on the constraint ability of helical wire at s=4s0 (W=0.03m, H=0.005m, α=π/4, a=0.4, b=0.9,F_t (0) =1N, and $F_b(0)=F_n(0)=0$N)*

Now consider several cases which illustrate the role of some parameters affecting the constraint ability. To characterize the effects of initial tangential force, results of constraint ability on the length of 4 pitches (4s0) are shown in Figure 5-A, while varying the radius of cylinder from 0.05m to 0.125m. Clearly, the length of 4 pitches is proportional to the radius. Although the constraint ability for each case increases with the growing radius, the case of smallest initial force $F_t(0)=0.1N$ has the fastest growth rate. It is well known that, compared to the largest initial force $F_t(0)=100N$, the friction force is relatively small and cannot easily dominate the constraint ability. Figure 5-B indicates that external pressure σ_p ranging from 0 to 100Pa almost does not influence the constraint ability at s=4s0 for a case of relatively large initial tangential force $F_t(0)$, however, for same external pressure, the smaller the initial force, the greater the constraint ability. In summary, situation of smaller $F_t(0)$ is more sensitive on radius and external pressure.

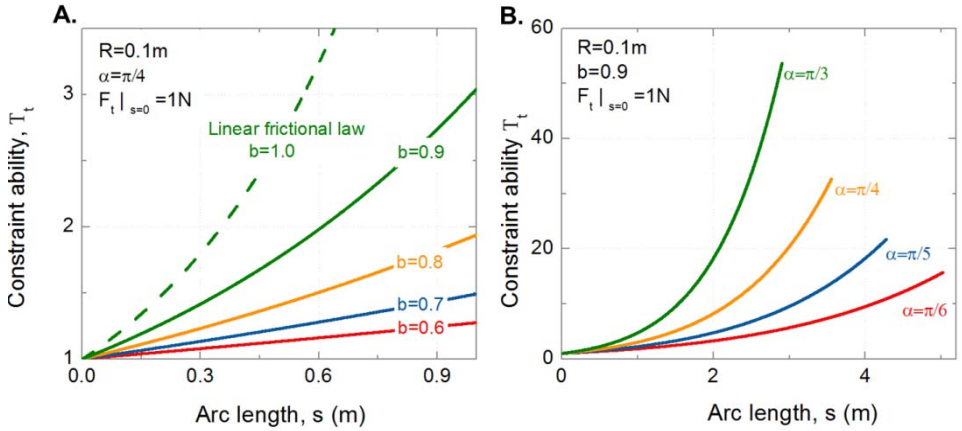

Figure 6: *Effect of frictional parameter and helical angle on the constraint ability of helical wire (W=0.03m, H=0.005m, a=0.4,F_t (0) =1N, $F_b(0)=F_n(0)=0N$, A:α=π/4, B:b=0.9)*

The third strong factor affecting the constraint ability is coefficient parameter *b*, which is readily related to the contact situation between wire and cylinder. The constraint ability increases with a rise of frictional parameter *b*. It has the largest value when linear frictional law is considered in the model.

Not less important than the influence of frictional parameter is the effect of helical angle. The variation of the constraint ability T_t with arc length s for different values of α is shown in Figure 6-B. At the same arc length, the larger the helical angle is, the higher is the constraint ability. This conclusion can also be derived from Eq.(9-a) where all gradient growth of force components maintain monotonically increasing relationship with helical angle. That is why, shown in Figure 6-B, the constraint ability at α=π/3 increases faster than the other three smaller α.

Shown in Figure 7, H and W, are geometric parameters of helical wire which affect the tangential and binormal constraint force. It is seen that a thinner wire can provide a larger tangential constraint force F_t. In contrary, higher binormal constraint force F_b needs a thicker wire. When the thickness rises from H=0.005m to H=0.010m and 0.015m, the tangential constraint force at s=4s0 will be reduced 6.2% and 12.1% respectively, while the binormal constraint force will increase 89.6% and 169.5%. In a word, influence of thickness on F_b appears to be greater than on F_t.

Unlike the influence of thickness on F_t and F_b, increasing the width of helical wire can improve both constraint forces. The changes in constraint force will be more obvious if an external pressure is applied on a wider wire.

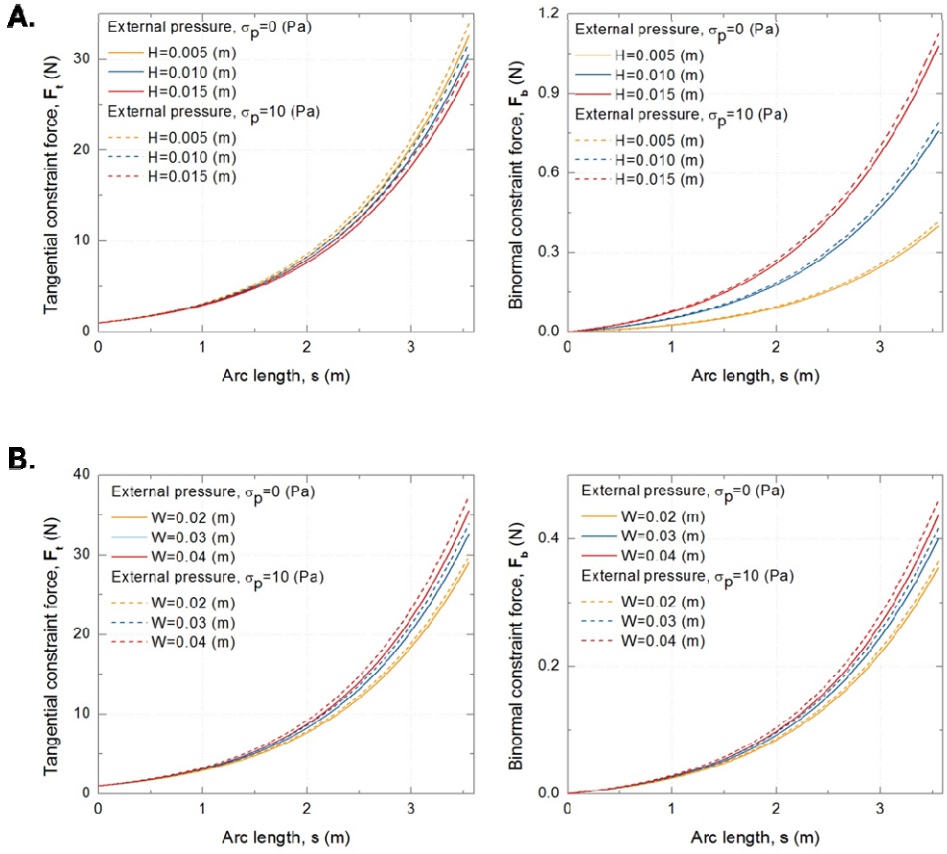

Figure 7: *Effect of thickness and width of helical wire on constant force components (R=0.1m,α=π/4, a=0.4,b=0.9, F_t (0) =1N,$F_b(0)=F_n(0)=0$N, A: W=0.03m; B: H=0.005m)*

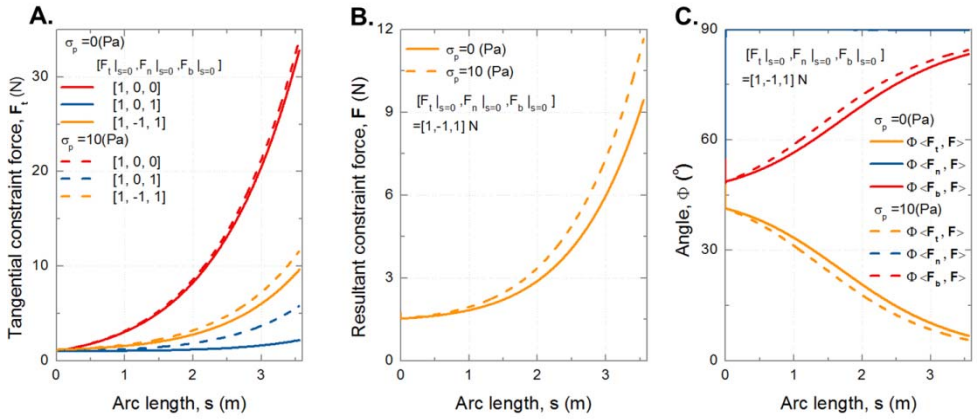

Figure 8: *Effect of different kinds of initial force components on the constraint force (W=0.03m, H=0.005m, R=0.1m, α=π/4, a=0.4, b=0.9)*

In this three-dimensional model, the type of initial force cannot only include the nonzero initial tangential force $F_t(0)$, but also contain the other two non-zero force components as well. Results of tangential constraint force in case of three kinds of initial force are shown in Fig 8-A. Compared with the case of only $F_t(0)$, either initial normal force or binormal force is applied, the constraint tangential force F_t can be significantly reduced. The blue lines correspond to the results of applying tangential and binormal forces together, making it clear that the tangential constraint force nearly does not increase along wire arc length unless when applying an external pressure. On base of this condition, if another initial normal force is added, the tangential constraint force will markedly increase, as shown by the orange lines in Fig 8-A. Fig 8-B shows the resultant constraint force being essentially coincident with the tangential one, which again indicates that the binormal and normal constraint

forces are relatively small. This conclusion can also be indicated by the angle variation between force components and resultant, shown in Figure 8-C. As the arc length rises, the angle between binormal force and resultant force tends to 90 degree, while the angle between tangential force and resultant force is close to 0 degree.

2) Two layers consisting of several wires wound around a rigid cylinder

Suppose both external and internal wires have the same geometric (W=0.03m and H=0.005m) and frictional parameters (a=0.4 and b=0.9). Only tangential initial force is applied on the initial position s=0 and the other two components are zero. Solutions about constraint force component can also be given by means of 4th order Runge-Kutta numerical method for two cases: σ_p=0Pa and σ_p=100Pa, shown in Figure 9. Both tangential and binormal constraint forces in internal layer are much larger than the one in external layer due to the "external pressure" generated by the external layer.

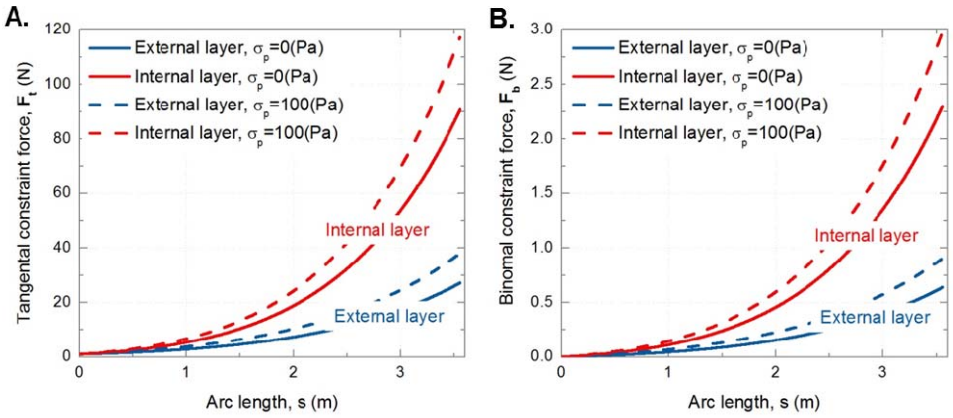

Figure 9: *Constraint force components of supposed helical wire (W=0.03m, H=0.005m, R=0.1m, α=π/4, a=0.4, b=0.9, F_t (0) =1N, $F_b(0)=F_n(0)=0$N)*

4 CONCLUSIONS

On basis of Clebsch-Kirchhoff equilibrium equations, a new three-dimensional model accurately taking into account the bending rigidity, non-linear frictional law and external pressure has been proposed for capstan problem, suitable for a wide range of engineering applications. Compared to existing models, it not only provides the tangential force characterizing the constraint ability of a helical wire wound around a rigid cylinder, but normal and binormal constraint forces can also be observed. Meanwhile, as regard to the external pressure, this model can be improved to evaluate the constraint ability of overlapped helical wires in a composite structure. According to the formulation of this three-dimensional model, many parameters which are relevant to geometry, friction law and initial force conditions can be important to determine the constraint ability. To distinguish these parametrical effects, numerous case studies are carried out. Results show that thicker wires can offer larger binormal constraint forces, but the tangential forces are reduced, i.e. the system constraint ability is compromised. Wider wire is beneficial to improve both tangential and binormal constraint forces. In addition, although applying external pressure indeed enables the helical wire to increase the constraint ability, its effectiveness critically depends on the initial force conditions. Especially, the case of only smaller initial tangential force is substantially influenced. Likewise, the constraint ability grows with increasing cylinder radius, frictional coefficients, as well as the wire helical angle which, of course, should be located at a suitable range for the functional integrity. It is evident that both cross-section wire size and helical angle are of importance for achieving accurate results. Thus, the deformation of wire along the arc length including cross-section and helical angle must be further considered. It should be noted that even though only wires with rectangular cross sections have been considered in this model, however, the constraint ability of circular cross sections can be also easily obtained by equivalently transferring its geometric parameters. For example, assume the diameter of a circular cross section is d, so the constraint ability of a yarn can be calculated by just replacing the parameters in the model as follows: H=d and W=ad ($0<a<\pi d/2$). Finally, despite the fact that this new three-dimensional model is able to predict the constraint ability of the structure based on capstan effects and that two-dimensional formula, similar to a model presented and assessed by experiment in Gao et al. [18], may be derived from this 3D model, it still needs experimental assessment and verification.

ACKNOWLEDGEMENTS

The authors acknowledge the support from the China National Key Research and Development Plan (Grant No.2016YFC0303702), Science Foundation of China University of Petroleum, Beijing (No.2462017YJRC040), the National Council of Scientific and Technological Development (CNPq), and the Brazil National Petroleum Agency (ANP) for this work.

References

[1]. Ramos R, Pesce C P. A consistent analytical model to predict the structural behaviour of flexible risers subjected to combined loads//ASME 2002 21st International Conference on Offshore Mechanics and Arctic Engineering. American Society of Mechanical Engineers, 2002: 141-148.

[2]. Ramos R, Kawano A. Local structural analysis of flexible pipes subjected to traction, torsion and pressure loads. Marine Structures, 2015, 42: 95-114.

[3]. Sævik S. Theoretical and experimental studies of stresses in flexible pipes. Computers & Structures, 2011, 89(23): 2273-2291.

[4]. Vaz M A, Rizzo N A S. A finite element model for flexible pipe armor wire instability. Marine Structures, 2011, 24(3): 275-291.

[5]. Attaway SW. The mechanics of friction in rope rescue. International Technical Rescue Symposium, 1999.

[6]. Werkmeister J, Slocum A. Theoretical and experimental determination of capstan drive stiffness. Precision Engineering 2007;31(1):55–67.

[7]. Tu C F, Fort T.A study of fiber–capstan friction. 1. Stribeck curves. Tribology International, 2004, 37(9): 701-710.

[8]. Tu C F, Fort T. A study of fiber-capstan friction. 2. Stick–slip phenomena. Tribology International, 2004, 37(9): 711-719.

[9]. Martin AJP, Mittelmann R. Some measurements of the friction of wool and mohair. J Textile Inst 1946:T269–80.

[10]. Howell HG. The general case of friction of a string round a cylinder. J Textile Inst 1953;44(8):359–62.

[11]. Howell HG. The friction of a fiber round a cylinder and itsdependence upon cylinder radius. J Textile Inst 1954;45(8):359–62.

[12]. Brown I F, Burgoyne C J. The friction and wear of Kevlar 49 sliding against aluminium at low velocity under high contact pressures. Wear, 1999, 236(1): 315-327.

[13]. Stuart JM. Capstan equation for strings with rigidity. Br J Appl.Phys,1961;12:559–62.

[14]. Wei M, Chen R. An improved capstan equation for nonflexible fibers and yarns. Textile Res J 1998;68(7):487–92.

[15]. Jung JH, Pan N, Kang TJ. Tension transmission via an elastic rod gripped by two circular-edged plates. International Journal of Mechanic Science 2007;49:1095–103.

[16]. Jung J H, Pan N, Kang T J. Capstan equation including bending rigidity and non-linear frictional behavior. Mechanism and Machine Theory, 2008, 43(6): 661-675.

[17]. Jung J H, Pan N, Kang T J. Generalized capstan problem: Bending rigidity, nonlinear friction, and extensibility effect. Tribology International, 2008, 41(6): 524-534.

[18]. Gao X, Wang L, Hao X. An improved capstan equation including power-law friction and bending rigidity for high performance yarn. Mechanism and Machine Theory, 2015, 90: 84-94.

[19]. Liu J, Vaz M A. Constraint ability of superposed woven fabrics wound on capstan. Mechanism and Machine Theory, 2016, 104: 303-312.

[20]. Love A E H.A treatise on the mathematical theory of elasticity. Cambridge University Press, 1944.

[21]. Reissner E. On finite deformations of space-curved beams. J Appl Math Phys(ZAMP), 1981, 32(6):734-744.

[22]. Liu J, Vaz M A, Custódio A B. Recovery length of high strength tapes in damaged flexible pipes. Ocean Engineering, 2016, 122: 1-9.